

Unbiased particle conformation extraction from scattering spectra using orthonormal basis expansions

Guan-Rong Huang,^{a*} Yangyang Wang,^b Yuya Shinohara,^c Lionel Porcar,^d Changwoo Do,^e William T. Heller^e and Wei-Ren Chen^{e*}

Received 15 August 2023

Accepted 31 December 2023

Edited by T. J. Sato, Tohoku University, Japan

Keywords: small-angle scattering; orthonormal basis expansion; particle density profiles; soft-matter systems.

^aDepartment of Materials and Optoelectronic Science, National Sun Yat-sen University, Kaohsiung 80424, Taiwan, ^bCenter for Nanophase Materials Sciences, Oak Ridge National Laboratory, Oak Ridge, TN 37831, USA, ^cMaterials Science and Technology Division, Oak Ridge National Laboratory, Oak Ridge, TN 37831, USA, ^dInstitut Laue–Langevin, BP 156, F-38042 Grenoble Cedex 9, France, and ^eNeutron Scattering Division, Oak Ridge National Laboratory, Oak Ridge, TN 37831, USA. *Correspondence e-mail: huangrn@mail.nsysu.edu.tw, chenw@ornl.gov

A strategy is outlined for quantitatively evaluating the particle density profiles from small-angle scattering spectra of dilute solutions. The approach employs an orthonormal basis function expansion method, enabling the determination of characteristic mass distributions in self-assembled structures without the need for a specific structural model. Through computational benchmarking, the efficacy of this approach is validated by effectively reconstructing the density profile of soft-ball systems with varying fuzziness from their scattering signatures. The feasibility of the method is demonstrated by fitting small-angle neutron scattering data obtained from Pluronic L64 micelles at different temperatures. This proposed approach is both simple and analytical, eliminating the requirement for a presumptive structural model in scattering analysis. The new method could therefore facilitate quantitative descriptions of complex nanoscopic structures inherent to numerous soft-matter systems using small-angle scattering techniques.

1. Introduction

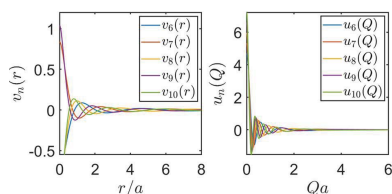
Small-angle scattering is a principal technique for the structural characterization of soft materials at the molecular level. For example, it is often used in structural investigations of dilute dispersion systems such as colloidal suspensions or micellar solutions, where a collection of ‘particles’ are suspended in ‘structureless’ solvent. The volume-normalized absolute scattering intensity $I(\mathbf{Q})$ from small-angle neutron scattering (SANS) by such a dilute system is directly related to the *excess* scattering length density (SLD) profile of the particle $\Delta\rho(\mathbf{r})$ as

$$I(\mathbf{Q}) = n_m |F(\mathbf{Q})|^2 + I_{\text{inc}} = n_m \left[\int_V \exp(-i\mathbf{Q} \cdot \mathbf{r}) \Delta\rho(\mathbf{r}) \, d\mathbf{r} \right]^2 + I_{\text{inc}}, \quad (1)$$

where I_{inc} is the incoherent background, $Q = |\mathbf{Q}| = (4\pi/\lambda)\sin(\theta/2)$, where θ is the scattering angle and λ is the wavelength of the incident radiation [Added definition OK?], and the excess SLD is given by the difference between the SLD profile of the particle $\rho_p(\mathbf{r})$ and the SLD of the solvent ρ_s ,

$$\Delta\rho(\mathbf{r}) \equiv \rho_p(\mathbf{r}) - \rho_s. \quad (2)$$

n_m is the number density of the particles (molecules). $\rho_p(\mathbf{r})$ can be explicitly expressed as $\rho_p(\mathbf{r}) = \sum_j b_j \delta(\mathbf{r} - \mathbf{x}_j)$. Here, the summation is over all constituent atoms of the particle. b_j is



the bound scattering length that represents the scattering properties of an atomic species under the condition of low incident neutron energy (Fermi & Marshall, 1947; Marshall & Lovesey, 1971; Yip, 2015). $\delta(x)$ is the Dirac delta function and \mathbf{x}_j is the position of j th atom. In the mean-field limit, $\rho_s \equiv \sum_j b_j/v_s$, where the summation is over the constituent atoms of the solvent molecule and v_s is the molecular volume of the solvent.

The scattering amplitude $F(\mathbf{Q})$ and excess SLD distribution $\Delta\rho(\mathbf{r})$ are related by the Fourier transform (Glatter, 2002)

$$F(\mathbf{Q}) = \int_V \exp(-i\mathbf{Q} \cdot \mathbf{r}) \Delta\rho(\mathbf{r}) d\mathbf{r}. \quad (3)$$

In this work, we consider only *isotropic* suspensions (solutions), so that neither $F(\mathbf{Q})$ nor $\Delta\rho(\mathbf{r})$ should depend on the solid angle. The Fourier transform of these radially symmetric functions in three-dimensional space boils down to the following integral:

$$F(Q) = 4\pi \int_0^\infty \Delta\rho(r) j_0(Qr) r^2 dr, \quad (4)$$

where $j_0(x) = \sin(x)/x$ is the spherical Bessel function of order zero. In principle, the density profile $\Delta\rho(r)$ can be obtained from the inverse Fourier transform of $F(Q)$,

$$\Delta\rho(r) = \frac{1}{2\pi^2} \int_0^\infty F(Q) j_0(Qr) Q^2 dQ. \quad (5)$$

In practice, however, a direct implementation of equation (5) is often not feasible, due to the limited Q range and the noise in the experimental data.

An intimately connected problem is the determination of the spatial autocorrelation function $\gamma(\mathbf{r})$ of the excess SLD from the inverse Fourier transform of the coherent scattering intensity $I(\mathbf{Q})$,

$$\gamma(\mathbf{r}) = \frac{V}{8\pi^3} \int \exp(i\mathbf{Q} \cdot \mathbf{r}) I(\mathbf{Q}) d\mathbf{Q}, \quad (6)$$

where

$$\gamma(\mathbf{r}) \equiv \int_V \Delta\rho(\mathbf{r}_1) \Delta\rho(\mathbf{r}_1 + \mathbf{r}) d\mathbf{r}_1. \quad (7)$$

Similarly, a direct inversion is generally impractical. As a result, several ‘indirect’ Fourier transform (IFT) methods have been proposed (Glatter, 2002, 1977; Moore, 1980; Hansen & Pedersen, 1991) by expanding the real-space distribution functions [e.g. the pair distance distribution function $p(r) \equiv \gamma(r)r^2$] and thereby the scattering intensity in terms of a series of basis functions.

Alternatively, the small-angle scattering spectra of dilute suspensions can also be analysed with simple structural models with *a priori* selected parameters. For example, these form-factor models include the homogeneous hard-sphere (Goldmints *et al.*, 1999, 1997; Stellbrink *et al.*, 1995) and ellipsoid models (Hassan *et al.*, 2003; Gapiński *et al.*, 2010;

Jensen *et al.*, 2013; Pedersen, 2000; Bergström & Pedersen, 1999), the inhomogeneous core-shell model (Hayter & Zemb, 1982; Zemb & Charpin, 1985; Cabane *et al.*, 1985; Sheu & Chen, 1988; Liu *et al.*, 1994, 1996; Svensson *et al.*, 1999; Willner *et al.*, 2000b; Adelsberger *et al.*, 2010; Manet *et al.*, 2011; König *et al.*, 2019), the core-corona model (Pedersen & Gerstenberg, 1996; Pedersen, 1994; Ramzi *et al.*, 1997; Liu *et al.*, 1998; Yang & Alexandridis, 2000; Yang *et al.*, 2000; Mao *et al.*, 2001; Castelletto *et al.*, 2002; Pedersen *et al.*, 2003; Bang *et al.*, 2004; Castelletto *et al.*, 2004; Choi *et al.*, 2009; Ma & Lodge, 2016; Zhao *et al.*, 2018; Wang *et al.*, 2018) and the fuzzy-sphere model (Poppe *et al.*, 1997; Chen *et al.*, 2007; Laurati *et al.*, 2007; Liu *et al.*, 2010; Li *et al.*, 2010; Huang *et al.*, 2020; Tung *et al.*, 2021), as well as phenomenological composite scattering functions which account for asymptotic scattering features from particles on different length scales (Brasher & Kaler, 1996; Hammouda, 2010a,b; Kumi *et al.*, 2014; Dozier *et al.*, 1991; Likos *et al.*, 1998; Willner *et al.*, 2000a). While such a model-based analysis enables the extraction of structural parameters of interest directly from the fitting, the results are highly dependent on the choice of the model.

In this work, we propose an alternative IFT approach that differs from the existing ones in the following ways. First, instead of analysing the pair correlation functions such as $\gamma(r)$ and $p(r)$, we focus on the excess SLD distribution $\Delta\rho(r)$, which is straightforward to interpret and contains crucial structural information such as particle size, geometric shape and inhomogeneous intra-particle mass distribution. The conventional IFT approach necessitates an additional step for deconvoluting the pair correlation function to obtain $\Delta\rho(r)$, which in turn complicates the process of error estimation for $\Delta\rho(r)$. Second, we expand the excess SLD profile $\Delta\rho(r)$ and scattering amplitude $F(Q)$ in terms of *orthogonal* **[Should this be orthonormal?]** basis functions. In this context, we note that function expansion is a frequently adopted strategy in ill-posed inverse problems. For example, an eigenfunction expansion method has been introduced to resolve relaxation time distributions from dynamic light scattering spectra (Provencher, 1976). The danger of obtaining incorrect solutions from non-orthogonal basis expansions has long been recognized for inverse problems in general. However, such a potential issue has been overlooked in the previously proposed IFT approaches to small-angle scattering spectra (Glatter, 2002, 1977; Moore, 1980; Hansen & Pedersen, 1991). This work attempts to remedy this problem by employing an orthonormal basis function expansion (Arfken *et al.*, 2012) to determine the SLD profile from SANS experiments. An obvious advantage of such a basis function expansion approach is that once the orthonormal basis functions are properly constructed, the regression analyses will be conducted in the vector space spanned by the unit vectors of transformed variables without relying on parametric equations based on specific structural assumptions.

The rest of this paper is organized as follows. In Section 2 we introduce the method of orthonormal eigenfunction expansion and review the basic properties of the expansion. The framework is subsequently applied to the construction of

orthonormal basis functions in Section 3. A numerical benchmark of soft-ball systems with varying fuzziness verifies the efficacy of this approach in Section 4. Finally, a SANS case study of micellar conformation at different temperatures is reported in Section 5 to provide support for the usefulness of this model-free approach. The constructed orthonormal basis functions are given in Appendix A. The imposition of maximized entropy to facilitate the implementation of basis expansions for spectral analysis is outlined in Appendix B.

2. The method of orthonormal basis expansion and its fundamental properties

The reconstruction of $\Delta\rho(r)$ can be accomplished by analysing $I(Q)$ in reciprocal space with the method of orthonormal eigenfunction expansion in the following steps. At first, we can expand $\sqrt{n_m}F(Q)$ and $\sqrt{n_m}\Delta\rho(r)$ as a linear combination of orthonormal basis functions with compatible boundary conditions (BCs),

$$\sqrt{n_m}F(Q) = \sum_{n=1}^{\infty} a_n u_n(Q), \quad \sqrt{n_m}\Delta\rho(r) = \sum_{n=1}^{\infty} b_n v_n(r), \quad (8)$$

where the basis functions in reciprocal and real space are denoted by $u_n(Q)$ and $v_n(r)$, respectively, a_n and b_n are the corresponding expansion coefficients, n is the integer index and r is the radial distance in spherical coordinates. $u_n(Q)$ and $v_n(r)$ are related straightforwardly by a pair of spherical Bessel transforms,

$$\begin{aligned} u_n(Q) &= \sqrt{\frac{2}{\pi}} \int dr r^2 v_n(r) j_0(Qr), \\ v_n(r) &= \sqrt{\frac{2}{\pi}} \int dQ Q^2 u_n(Q) j_0(Qr), \end{aligned} \quad (9)$$

where $j_0(x) = \sin x/x$ is the spherical Bessel function of order zero. Subsequently, a_n can be extracted by fitting the experimentally measured $I(Q)$ using equations (1) and (8). Because of the orthonormal properties, a_n is proportional to b_n up to a constant $\sqrt{8\pi^3}$, as shall be demonstrated later in this section. Therefore, we can use equation (8) to reconstruct $\sqrt{n_m}\Delta\rho(r)$ once the eigenfunctions and associated expansion coefficients are obtained. The speed of convergence of this procedure can be further accelerated by the constraint of maximum entropy (see Appendix B for more information),

$$\sqrt{n_m}F(Q) = \lambda_0 \left\{ \exp \left[\sum_{n=1}^{\infty} \lambda_n u_n(Q) \right] - 1 \right\}. \quad (10)$$

In comparison with equation (8), equation (10) would require fewer terms of $\{u_n(Q)\}$ for the regression analysis of $I(Q)$.

Now let us construct the fundamental relations among these expansion coefficients and eigen basis functions by the inner products of functional space spanned by $\{u_n(Q)\}$ and $\{v_n(r)\}$, which can be expressed as

$$\langle u_n(Q), u_m(Q) \rangle \equiv 4\pi \int_0^{\infty} dQ Q^2 u_n(Q) u_m(Q), \quad (11)$$

and

$$\langle v_n(r), v_m(r) \rangle \equiv 4\pi \int_0^{\infty} dr r^2 v_n(r) v_m(r). \quad (12)$$

[Does the subscript m now indicate a variable (and thus should be italic)? Or does it still indicate ‘molecule’ as in eqs. (1) and (8) (and thus should be upright)? Please clarify, here and elsewhere] The relationships between $u_n(Q)$ and $v_n(r)$ can be expressed in terms of their inner product with $j_0(Qr)$:

$$\begin{aligned} u_n(Q) &= \sqrt{\frac{2}{\pi}} \int_0^{\infty} dr r^2 v_n(r) j_0(Qr) \\ &= \sqrt{\frac{1}{8\pi^3}} \langle v_n(r), j_0(Qr) \rangle, \end{aligned} \quad (13)$$

and

$$\begin{aligned} v_n(r) &= \sqrt{\frac{2}{\pi}} \int_0^{\infty} dQ Q^2 u_n(Q) j_0(Qr) \\ &= \sqrt{\frac{1}{8\pi^3}} \langle u_n(Q), j_0(Qr) \rangle. \end{aligned} \quad (14)$$

According to equations (11) and (12), the inner products in real space are identical to those in reciprocal space. Explicitly, we have

$$\begin{aligned} \langle v_n(r), v_m(r) \rangle &= 8 \int_0^{\infty} \int_0^{\infty} \int_0^{\infty} dQ dQ' dr Q^2 Q'^2 r^2 j_0(Qr) j_0(Q'r) \\ &\quad \times u_n(Q) u_m(Q') \\ &= 4\pi \int_0^{\infty} \int_0^{\infty} dQ dQ' Q^2 \delta(Q - Q') u_n(Q) u_m(Q') \\ &= 4\pi \int_0^{\infty} dQ Q^2 u_n(Q) u_m(Q) \\ &= \langle u_n(Q), u_m(Q) \rangle. \end{aligned} \quad (15)$$

In other words, if the basis functions $\{u_n(Q)\}$ are orthonormal in reciprocal space, so are $\{v_n(r)\}$ in real space,

$$\delta_{m,n} = \langle u_n(Q), u_m(Q) \rangle = \langle v_n(r), v_m(r) \rangle, \quad (16)$$

where $\delta_{m,n}$ is the Kronecker delta.

Based on the method of eigenfunction expansion, one can always expand any function $f(r)$ in terms of $\{v_n(r)\}$ with compatible boundary conditions (BCs) as

$$f(r) = \sum_n b_n v_n(r), \quad (17)$$

where the expansion coefficient b_n associated with the basis function $v_n(r)$ is found to be

$$b_n = \langle v_n(r), f(r) \rangle. \tag{18}$$

Similarly, the Fourier transform of $f(r)$ can be expanded as

$$\begin{aligned} \tilde{f}(Q) &= 4\pi \int_0^\infty dr r^2 f(r) j_0(Qr) \\ &= \sum_n a_n u_n(Q), \end{aligned} \tag{19}$$

and the expansion coefficient a_n associated with $u_n(Q)$ is

$$a_n = \langle u_n(Q), \tilde{f}(Q) \rangle. \tag{20}$$

As a result of the orthonormality condition, one can further relate a_n to b_n as

$$\begin{aligned} a_n &= \left\langle u_n(Q), 4\pi \int_0^\infty dr r^2 f(r) j_0(Qr) \right\rangle \\ &= \langle u_n(Q), \langle f(r), j_0(Qr) \rangle \rangle \\ &= \sum_m b_m \langle u_n(Q), \langle v_m(r), j_0(Qr) \rangle \rangle \\ &= \sqrt{8\pi^3} \sum_m b_m \langle u_n(Q), u_m(Q) \rangle \\ &= \sqrt{8\pi^3} \sum_m b_m \delta_{m,n} \\ &= \sqrt{8\pi^3} b_n. \end{aligned} \tag{21}$$

Equation (21) shows that a_n is linearly related to b_n with a proportionality constant of $\sqrt{8\pi^3}$. As a result, one only needs to calculate the coefficients in either reciprocal or real space in order to reconstruct $f(r)$ or $\tilde{f}(Q)$.

3. Construction of the analytical orthonormal basis functions

To ensure convergence of the expansion, the BCs of the orthonormal basis functions should be compatible with those of the target functions. In the current case, the derivatives of the basis functions $u_n(Q)$ or $v_n(r)$ at the origin and infinity must be zero. In general soft-matter systems, $\Delta\rho(r)$ can be normalized and the radius of gyration R_g is finite. Therefore, the corresponding BCs for the scattering amplitude are $F'(0) = 0$ and $F'(\infty) = 0$, being the natural characteristics of the kinds of system under study. Given the mathematical properties of the two-point static correlation function, through which the structural information is rendered by scattering, the Lorentzian-like distributions $(1 + a^2 Q^2)^{-k}$ or $[1 + (r/a)^2]^{-k}$ are found to meet the BCs of coherent scattering, where k is a positive integer and a is simply a constant with the dimension of length. To obtain the orthonormal set, the Gram-Schmidt process is adopted over this distribution with different values of k . Without losing generality, $u_1(Q)$ is chosen to be

$$\begin{aligned} u_1(Q) &= \frac{(1 + a^2 Q^2)^{-k}}{\sqrt{\langle (1 + a^2 Q^2)^{-k}, (1 + a^2 Q^2)^{-k} \rangle}} \\ &= \frac{1}{\sqrt{I_{2k}}} (1 + a^2 Q^2)^{-k}, \end{aligned} \tag{22}$$

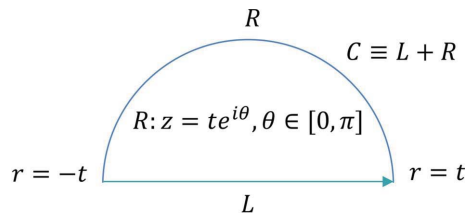


Figure 1 The closed loop on the complex plane for carrying out the integral of equation (24).

where I_x is defined by the Euler gamma function $\Gamma(x)$ as

$$I_x \equiv \frac{\sqrt{\pi^3}}{a^3} \frac{\Gamma[x - (3/2)]}{\Gamma(x)}. \tag{23}$$

Equation (22) can be transformed using equation (14) and the result is

$$\begin{aligned} v_1(r) &= \sqrt{\frac{2}{\pi I_{2k}}} \int_0^\infty dQ Q^2 (1 + a^2 Q^2)^{-k} j_0(Qr) \\ &= \sqrt{\frac{2}{\pi I_{2k}}} \frac{1}{r} \int_0^\infty dQ \frac{Q \sin(Qr)}{(1 + a^2 Q^2)^k} \\ &= -\sqrt{\frac{1}{2\pi a^2 I_{2k}}} \frac{1}{r} \frac{d}{dr} \lim_{t \rightarrow \infty} \left[\int_{-t}^t dQ \frac{\cos(Qr/a)}{(1 + Q^2)^k} \right]. \end{aligned} \tag{24}$$

To obtain the analytical expression of the integral of equation (24), the Cauchy integral theorem on a closed loop over a complex plane is adopted, as indicated by Fig. 1. The loop $C \equiv R + L$ which encloses the pole of $z = i$ is selected. The integration over arc R approaches zero since

$$\lim_{t \rightarrow \infty} \frac{\pi t}{(t^2 - 1)^k} = 0 \text{ for } k > \frac{1}{2}. \tag{25}$$

Therefore, the final expression of $v_1(r)$ is given by

$$v_1(r) = \frac{1}{i(k-1)!} \sqrt{\frac{2\pi}{a^2 I_{2k}}} \frac{1}{r} \frac{d}{dr} \left\{ \frac{d^{k-1}}{dQ^{k-1}} \left[\frac{\exp(iQr/a)}{(Q+i)^k} \right]_{Q=i} \right\}. \tag{26}$$

Likewise,

$$\begin{aligned}
 U_2(Q) &= \frac{(1 + a^2 Q^2)^{-k-1}}{\sqrt{I_{2k+2}}} - \langle u_1(Q), \frac{(1 + a^2 Q^2)^{-k-1}}{\sqrt{I_{2k+2}}} \rangle, \\
 u_2(Q) &= \frac{U_2(Q)}{\sqrt{\langle U_2(Q), U_2(Q) \rangle}}, \\
 &\vdots \\
 U_l(Q) &= \frac{(1 + a^2 Q^2)^{-k-l+1}}{\sqrt{I_{2k+2l-2}}} - \sum_{m=1}^{l-1} \langle u_m(Q), \frac{(1 + a^2 Q^2)^{-k-l+1}}{\sqrt{I_{2k+2l-2}}} \rangle, \\
 u_l(Q) &= \frac{U_l(Q)}{\sqrt{\langle U_l(Q), U_l(Q) \rangle}}.
 \end{aligned}
 \tag{27}$$

The expression of $\{v_1(r), v_2(r), \dots, v_l(r)\}$ can clearly be calculated analytically by transforming $\{u_1(Q), u_2(Q), \dots, u_l(Q)\}$ via equations (14) and (26). It is instructive to point out that $u_n(Q)$ and $v_n(r)$ can be interchanged to meet the required compatibility of BCs inherent to the data. For example, the Fourier transform pair $u_n(Q)$ and $v_n(r)$ can be replaced by $v_n(Q)$ and $u_n(r)$ to meet the BCs of a real-space function $f(r)$ which are $f'(0) = 0$ and $f'(\infty) = 0$. The ten basis functions of $\{u_n(Q)\}$ and $\{v_n(r)\}$ are given in Appendix A.

4. A computational benchmark: density profile reconstruction of soft-sphere systems with varying fuzziness

In this section, we evaluate the effectiveness of the orthonormal basis expansion method by analysing the scattering intensities of soft-sphere systems with a fixed radius $R = 50 \text{ \AA}$, but varying levels of fuzziness characterized by $s = 20, 30$ and 40 \AA . Soft spheres in the fuzziness regime exhibit a complex mixture of molecular constituents with solvent molecules, leading to a density profile that is non-zero everywhere and lacks a specific radial boundary. To analyse the scattering behaviour quantitatively, we employ the dimensionless form factor $P(Q)$, expressed analytically as (Stieger *et al.*, 2004)

$$P(Q) = \frac{9[\sin(QR) - QR \cos(QR)]^2}{(QR)^6} \exp\left[\frac{-(sQ)^2}{2}\right], \tag{28}$$

where R represents the core radius and s denotes the corona radius fuzziness of the soft spheres. The normalized density profile, denoted $\Delta\rho(r)/(\Delta\rho\sqrt{n_m})$, is calculated using equation (5),

$$\begin{aligned}
 \frac{\Delta\rho(r)}{\Delta\rho\sqrt{n_m}} &= \frac{1}{2\pi^2 r} \int_0^\infty dQ Q \sin(Qr) \frac{3[\sin(QR) - QR \cos(QR)]}{(QR)^3} \\
 &\times \exp\left[\frac{-(sQ)^2}{4}\right].
 \end{aligned}
 \tag{29}$$

Fig. 2 presents a comparison between the numerical ground truth (represented by blue solid lines) obtained from equa-

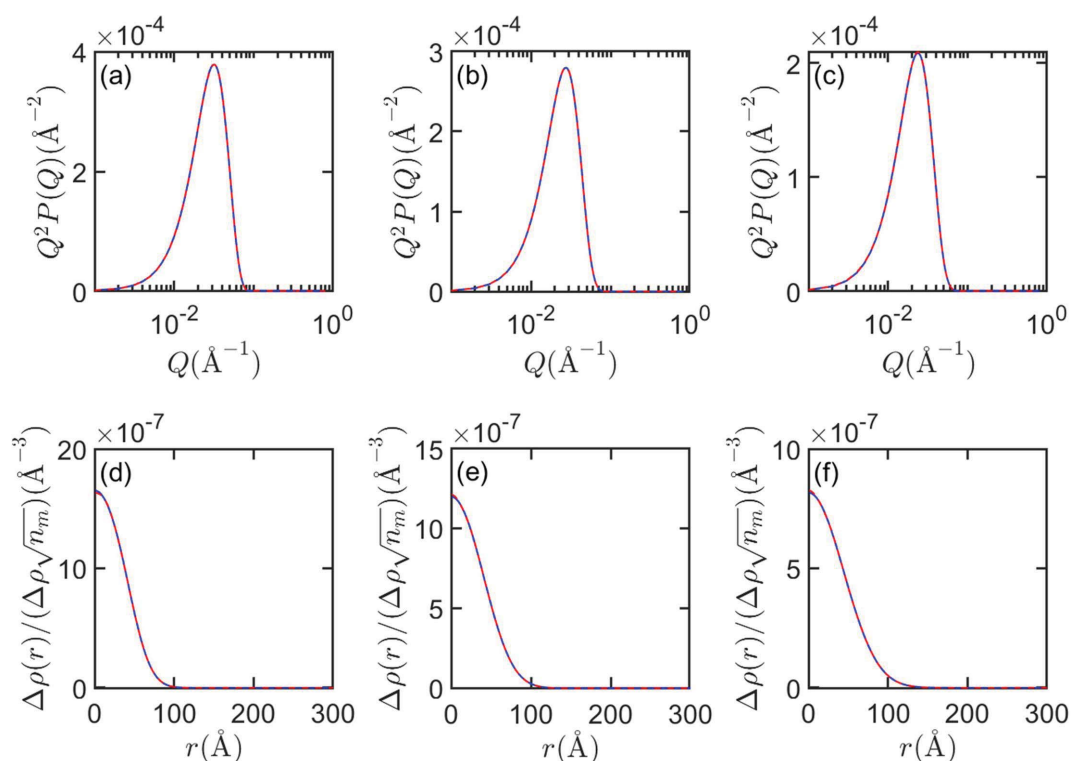


Figure 2

The numerical benchmark between the analytical model obtained by equations (28) and (29) and its model fitting by equation (8) for soft-ball systems of core radius $R = 50 \text{ \AA}$ at different radius fuzziness. Panels (a), (b) and (c) give comparisons in $Q^2 P(Q)$ in reciprocal space, while panels (d), (e) and (f) display the corresponding normalized density profiles in real space. The radius fuzziness (s) for panels (a), (b) and (c) is 20 \AA , 30 \AA and 40 \AA , respectively.

tions (28) and (29), and the fitted curve (illustrated by red dashed lines) obtained using equation (8) and the orthonormal basis functions in Appendix A, with eight expansion terms employed. Overall, quantitative agreement between these curves in both real and reciprocal space is observed. This benchmark verifies the effectiveness of the orthonormal basis expansion method in accurately reconstructing the density profiles of soft-sphere systems with varying fuzziness.

It is important to mention that analytical scattering functions do not exist for several soft-matter systems. However, the strength of the proposed method lies in its versatility, as it is not restricted to specific types of scattering functions. Consequently, this method becomes valuable for extracting density profiles from experimentally measured scattering intensities, providing a useful tool for investigating and understanding the structural complexities of such soft-matter systems.

5. An illustrative example: structure of triblock copolymer micelles in aqueous solution investigated by SANS

We further demonstrate the feasibility of our proposed approach using SANS data obtained from aqueous solutions of Pluronic L64 as an example. Previous analyses of SANS data from L64 micelles have traditionally involved various conventional analytical models (Liu *et al.*, 1998; Yang *et al.*, 2000; Mao *et al.*, 2001; Liu *et al.*, 1996; Svensson *et al.*, 1999; Goldmints *et al.*, 1999, 1997), including core-shell, ellipsoids, fuzzy soft balls and cape-and-gown. However, the absence of a unified framework for describing the structure of these micelles has led to challenges. It is conceivable that the scattering signatures may not align with the predictions of conventional scattering models.

Pluronic L64 is triblock copolymer that has 30 polypropylene oxide (PPO) middle blocks and 13 polyethylene oxide (PEO) end blocks [(PEO)₁₃(PPO)₃₀(PEO)₁₃], with a molecular weight of 2990 Da. Below the critical micelle temperature (CMT), both the PEO and PPO blocks are hydrophilic and the L64 chains readily dissolve in water as monomers. Upon increasing the temperature above the CMT, the hydrogen bonds between water and polymer molecules are disrupted and PPO tends to become less hydrophilic than PEO. As a result, a disparity of hydrophilicity is created between the end blocks and the middle block of the polymer chain. The copolymer molecules therefore acquire amphiphilic properties in an aqueous environment and self-assemble into micellar structures above the CMT-concentration line.

During the experiments the temperature stability was controlled to within $\pm 0.1^\circ\text{C}$. Samples with a fixed L64 concentration of 1 wt% and 2 wt% were prepared using D₂O. The prepared samples were further filtered using Anotop membrane filters (0.02 μm), mixed for 48 h and equilibrated for 24 h prior to experiment. SANS measurements were performed using the extended Q -range small-angle neutron scattering diffractometer (EQ-SANS) at the Spallation Neutron Source, Oak Ridge National Laboratory (Zhao *et al.*, 2010; Heller *et al.*, 2018), and the D22 large dynamic range small-angle diffractometer, Institut Laue-Langevin, Grenoble, France. The probed Q range was from 0.007 to 0.4 \AA^{-1} on the EQ-SANS beamline and from 0.003 to 0.6 \AA^{-1} on the D22 beamline. The samples were accommodated in Hellma cells with a 2 mm path length. The measured scattering intensities were corrected for the detector background, sensitivity and empty-cell scattering, and were normalized by the standard procedure in order to obtain the absolute intensities (Heller *et al.*, 2018; Arnold *et al.*, 2014).

Before presenting the details of the quantitative analysis, we first examine the qualitative features of the measured SANS

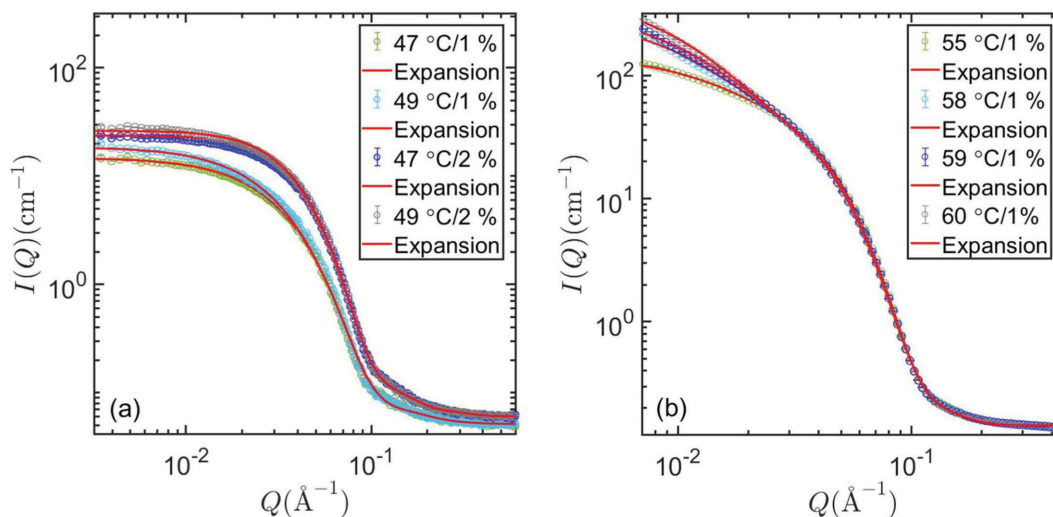


Figure 3 The SANS scattering differential cross section $I(Q)$ of L64 micellar solutions with 1 or 2 wt% concentration at six different temperatures. Experimental uncertainties are either comparable to or smaller than the symbol size. Model fitting curves (red solid lines) using equations (8) or (10), accounting for instrumental resolution, are compared with experimentally measured results (coloured circular symbols). A remarkable quantitative agreement is observed between the experimental data and the model curves. Panel (a) represents measurements conducted on EQ-SANS (Oak Ridge National Laboratory) and panel (b) shows data obtained on D22 (Institut Laue-Langevin).

spectra. Fig. 3 shows the SANS data obtained from the aqueous solutions of L64 at 1 wt% and 2 wt% at six different temperatures. These findings strongly support the notion that the measured scattering intensity $I(Q)$ primarily arises from intra-micellar spatial correlation, while the inter-micellar spatial correlation would have an insignificant impact on the subsequent data analysis. Consequently, we can infer that the same statement may also apply to the $I(Q)$ data presented in Fig. 3(b), even though the curves do not exhibit apparent flattening trends.

In what follows we present the implementation of the proposed basis expansion approach to determine the SLD distributions of the constituents of L64 micelles, including both $(\text{PEO})_{13}(\text{PPO})_{30}(\text{PEO})_{13}$ surfactant molecules and invasive water. The measured SANS absolute intensity $I(Q)$ of the L64 micellar solutions can be expressed by equation (1) (Chen, 1986). Similar to many amphiphiles in aqueous environments, the self-assembled structure of the L64 micelle is characterized by a densely packed core consisting of less hydrophilic PPO components surrounded by a more diffuse region composed of more polar PEO blocks. The density distribution of L64 molecules decays towards the periphery from the micellar core region. In addition, because of the difference in hydrophilicity of PEO and PPO when the temperature is higher than the CMT, the density profile of water penetration is inhomogeneous along the micellar radial direction, with more invasive water molecules residing at the core? than in the outer layer. Since the packing pattern of invasive water is different from that of bulk water, both the polymer segment and invasive water molecules should be considered constituents of the L64 micelle. Their contributions to the measured coherent scattering are, respectively, from compositional and density differences relative to bulk water.

As evident from equation (1), a quantitative description of the L64 micellar structure begins with an analysis of $\sqrt{n_m}F(Q)$. To this end we resort to the basis expansion method for analysing the scattering intensity $I(Q)$ using equations (8) and (10) given in Fig. 3. As a starting point, $\sqrt{n_m}F(Q)$ is first expanded based on the basis function given in Appendix A. The $\{a_n\}$ can be determined from measured spectra, and $\sqrt{n_m}\Delta\rho(r)$ can therefore be reconstructed by equation (8) and the identity $a_n = \sqrt{8\pi^3}b_n$, as demonstrated in equation (21).

An example of the implementation of the regression analysis based on our proposed strategy is given in Fig. 4. Complemented by the scheme of maximized entropy described in Appendix B, the experimentally measured $I(Q)$ (black circles) given in Fig. 4(a) can be approximated by a series of five basis functions using equation (10). The disagreement is around or within the experimental statistics errors. From the associated expansion coefficients given in Fig. 4(b), the quantity $\sqrt{n_m}\Delta\rho(r)$ can be reliably extracted from the measured $I(Q)$ without using a predetermined expression as the input.

In Figs. 5(a) and 5(b) we present the extracted $\sqrt{n_m}\Delta\rho(r)$ corresponding to the various $I(Q)$ given in Fig. 3. The results are further multiplied by r^2 to highlight the subtle structural features. From Figs. 5(c) and 5(d), the radial distribution of

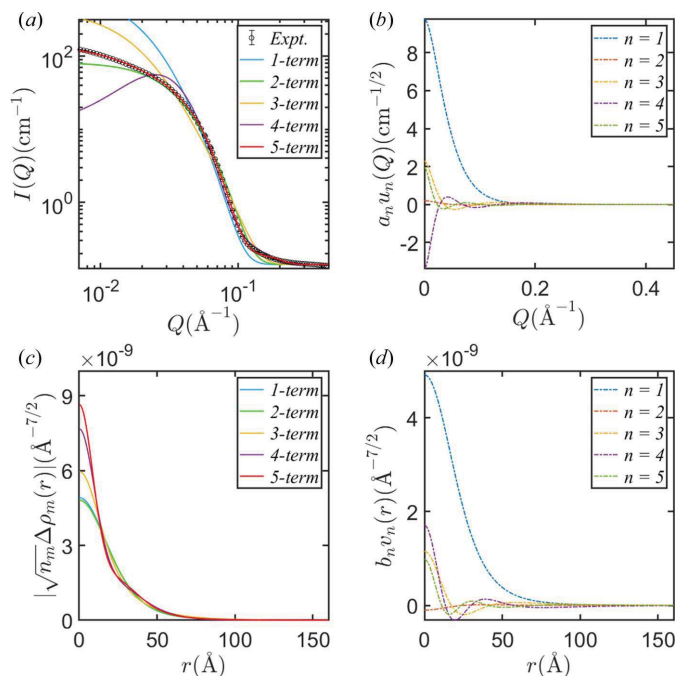


Figure 4

(a) $I(Q)$ corresponding to the L64 micellar solution at 55°C (black circles) is approximated by a series of five basis functions (red solid curve **Is this the convolution of the other coloured lines?**). The disagreement is around or within experimental error. (b) The expansion decomposition **curves?** from the corresponding five basis functions of $a_n u_n(Q)$. (c) The reconstructed $\sqrt{n_m}\Delta\rho(r)$ with different numbers of basis functions. (d) The expansion decomposition **curves?** from the corresponding five basis functions of $b_n v_n(r)$. a_n are linearly proportional to b_n .

$\sqrt{n_m}\Delta\rho(r)$ is characterized by the following features: a central core region ranging from $r = 0$ to approximately $r = 20$ Å, an intermediate region where a characteristic peak in $r^2\sqrt{n_m}\Delta\rho(r)$ is observed between $r = 40$ Å and $r = 50$ Å, and a micellar periphery region where $r > 80$ Å. Upon increasing the temperature, the mass distribution shifts progressively towards the outer shell, as shown in Figs. 5(c) and 5(d).

Because of the non-parametric nature of our proposed approach, the radially averaged characteristic variation in the radial distribution of $\sqrt{n_m}\Delta\rho(r)$ displayed in Figs. 5(a) and 5(b) is not artificially imposed by any pre-determined function as in the existing parametric approaches.

It is instructive to point out that the micelle number density n_m can be further independently determined using the scheme of contrast variation, as already demonstrated by existing SANS studies of micellar solutions (Li *et al.*, 2010; Huang *et al.*, 2020; Tung *et al.*, 2021). In the 2 wt% case of Fig. 5(b), the slight negative values of $r^2\sqrt{n_m}\Delta\rho(r)$ around the outer shell region, which are not observed in the 1 wt% case, could potentially be attributed to the slight inter-micellar interaction. Consequently, it is reasonable to infer that the overall aggregated size of L64 micelles would be smaller in the 2 wt% solution than in the 1 wt% solution.

To quantify the micelle size, a commonly used structural parameter can be employed: the radius of gyration R_g , which can be calculated using the following equation (Huang *et al.*, 2019):

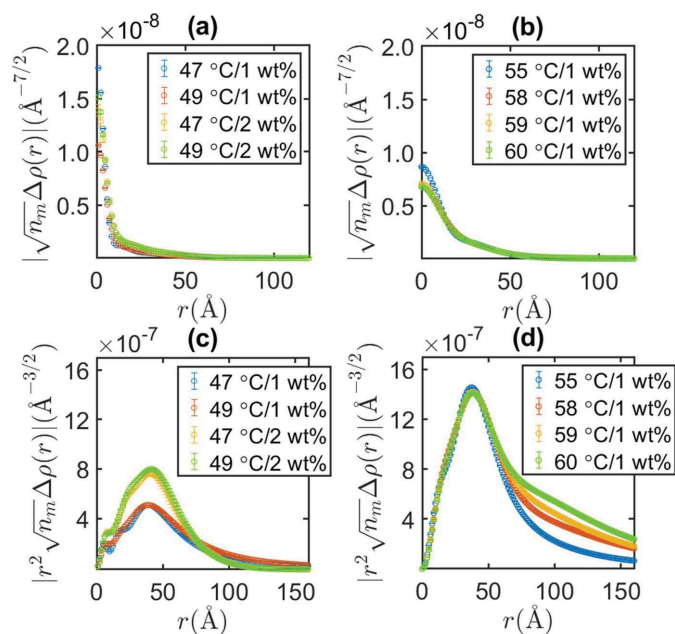


Figure 5
The radial distributions extracted from the $I(Q)$ in Fig. 3 using equations (10) and (21). (a) and (b) The profiles of $\sqrt{n_m}\Delta\rho(r)$. (c) and (d) The corresponding profiles of $r^2\sqrt{n_m}\Delta\rho(r)$.

$$R_g^2 = \frac{\int_0^\infty \Delta\rho(r) r^4 dr}{\int_0^\infty \Delta\rho(r) r^2 dr} = -\frac{1}{2} \nabla_Q^2 P(Q)|_{Q \rightarrow 0}, \quad (30)$$

where $P(Q)$ is the normalized form factor. Fig. 6 gives the R_g calculated from the results given in Fig. 5. As a quantitative measure of micellar size, R_g detects changes in the second moment of $r^2\Delta\rho(r)$ according to equation (30). A steady increase in R_g indicates an increase in micellar size upon raising the temperature. This size estimation is consistent with the findings reported previously (Liu *et al.*, 1998). This agreement provides further validation and confidence in the accuracy of our results, as it aligns with the established knowledge and understanding of the system's properties.

Lastly, it should be mentioned that equation (1) is primarily suitable for systems with insignificant size polydispersity. This aspect can be demonstrated by the following equation:

$$I(Q) = n_m \int dR |F(Q, R)|^2 f(R) + I_{\text{inc}} \neq n_m \left| \int dR F(Q, R) f(R) \right|^2 + I_{\text{inc}}, \quad (31)$$

where R and $f(R)$ represent the size and size distribution, respectively, of the self-assembled molecules. As evident from equation (31), equation (1) does not account for the cross-term contributions of scattering amplitudes, which could be significant when dealing with systems having a substantial size polydispersity. However, there is a mathematically tractable method that can potentially address this issue and extract the average SLD distribution. The central moment expansion method has been proposed to achieve this goal (Huang *et al.*, 2023). Using this method, the impact of size polydispersity on

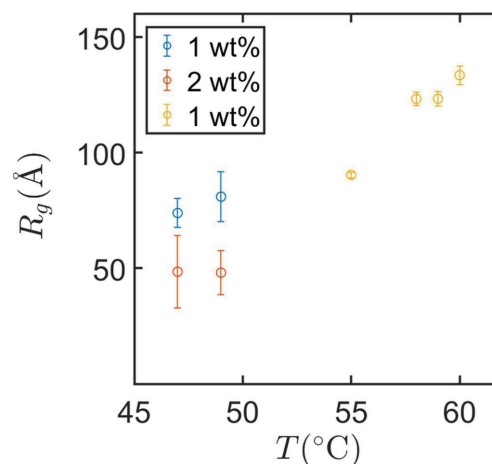


Figure 6
The calculated radius of gyration R_g with 1 or 2 wt% concentration as a function of temperature, using equation (30) and the distribution profiles in Fig. 5.

the scattering data could be appropriately considered, allowing for a more accurate determination of the average SLD distribution.

6. Concluding discussion

A basis function expansion approach has been developed for the quantitative evaluation of the structures of dilute soft-matter solutions from their small-angle neutron scattering spectra. This model-free method allows determination of the conformational characteristics of soft-matter systems without any pre-determined models, thus avoiding any potentially biased interpretations of experimental data.

Compared with the existing numerical procedures such as indirect Fourier transform (IFT) (Glatter, 2002, 1977; Moore, 1980; Hansen & Pedersen, 1991), the proposed method has several advantages in terms of accuracy, efficiency and applicability. First, the basis functions selected in our inverse scheme form a complete set, ensuring the uniqueness of solutions in regression analysis without the inclusion of any regularization term, whose optimal smooth parameter is normally chosen based on *a priori* knowledge of the investigated soft-matter systems (Svergun, 1992; Vada & Sager, 2011). Secondly, since our constructed basis functions can be expressed analytically, the accumulated numerical errors in the optimization process of spectral analysis can be significantly minimized. Thirdly, since our selected basis functions are also compatible with the boundary conditions inherent in the structures of the studied systems, faster convergence in determining the coefficients associated with the related basis functions is guaranteed. For example, the commonly used spline functions and Fourier sine basis, which have been used in scattering data analysis (Glatter, 1977; Moore, 1980), would normally require roughly fifty terms for a particle size of 50 Å to ensure convergence. Lastly, the existing IFT literature has not taken into account numerical uncertainties in the scattering length density (SLD) profile. Addressing these uncertainties would require an additional step of deconvolving the

pair density distribution function extracted from experimental data using IFT (Glatter, 2002; Grant, 2022). While a one-step IFT approach utilizing a quadratic matrix with respect to the components of SLD distributions has been proposed (Hansen, 2016), the aforementioned issues inherent in the IFT method still need to be addressed to avoid potential entrapment in multiple minima during the optimization process. It is therefore important to point out that the propagation of experimental errors in our basis expansion approach can be straightforwardly calculated through the related Jacobian matrix, since the expansion coefficients in reciprocal and real space differ only by a proportionality constant.

The prospects of the proposed approach to small-angle scattering data analysis are appealing: it can be used to examine the influence of invasive solvent molecules on conformational flexibility in various globular colloids with a molecular architecture open to solvent penetration. Because of the boundary condition compatibility and orthonormal properties, the self-assembly behaviours of particulate systems, such as wormlike and lamellar micelles, and non-particulate systems, such as microemulsions and porous materials whose structures lack spherical symmetry, can also be addressed based on an extension of the same expansion strategy. For instance, the extracted SLD profile can offer a mathematically tractable avenue for further particle shape analysis by either incorporating the spherical harmonic components (Svergun *et al.*, 1982) or accounting for the symmetries in the Fourier transform (Hansen, 2016). **Please add a callout for Fig. 7. It is currently not mentioned anywhere.**

APPENDIX A

The orthonormal sets of $\{u_n(Q)\}$ and $\{v_n(r)\}$

$$u_1(x) = \sqrt{\frac{1}{I_6}} x^3,$$

$$u_2(x) = \sqrt{\frac{22}{I_8}} \left(x^4 - \frac{3}{4} x^3 \right),$$

$$u_3(x) = \sqrt{\frac{364}{I_{10}}} \left(x^5 - \frac{11}{8} x^4 + \frac{99}{224} x^3 \right),$$

$$u_4(x) = \sqrt{\frac{38\,760}{7I_{12}}} \left(x^6 - \frac{39}{20} x^5 + \frac{143}{120} x^4 - \frac{143}{640} x^3 \right),$$

$$u_5(x) = \sqrt{\frac{81\,719}{I_{14}}} \left(x^7 - \frac{5}{2} x^6 + \frac{195}{88} x^5 - \frac{13}{16} x^4 + \frac{13}{128} x^3 \right),$$

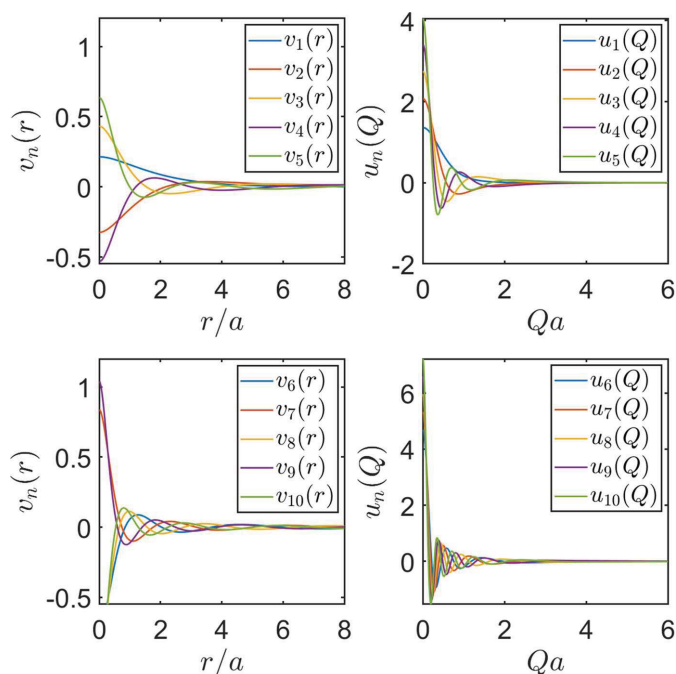


Figure 7
Plots of ten $\{u_n(Q)\}$ and $\{v_n(r)\}$ basis functions.

$$u_6(x) = \sqrt{\frac{1\,193\,010}{I_{16}}} \left(x^8 - \frac{85}{28} x^7 + \frac{1275}{364} x^6 - \frac{425}{224} x^5 + \frac{425}{896} x^4 - \frac{153}{3584} x^3 \right),$$

$$u_7(x) = \sqrt{\frac{17\,368\,680}{I_{18}}} \left(x^9 - \frac{57}{16} x^8 + \frac{323}{64} x^7 - \frac{1615}{448} x^6 + \frac{4845}{3584} x^5 - \frac{3553}{14\,336} x^4 + \frac{969}{57\,344} x^3 \right),$$

$$u_8(x) = \sqrt{\frac{253\,086\,480}{I_{20}}} \left(x^{10} - \frac{49}{12} x^9 + \frac{931}{136} x^8 - \frac{4655}{768} x^7 + \frac{4655}{1536} x^6 - \frac{1729}{2048} x^5 + \frac{1463}{12\,288} x^4 - \frac{209}{32\,768} x^3 \right),$$

$$u_9(x) = \sqrt{\frac{3\,697\,182\,450}{I_{22}}} \left(x^{11} - \frac{23}{5} x^{10} + \frac{3381}{380} x^9 - \frac{1127}{120} x^8 + \frac{1127}{192} x^7 - \frac{1127}{512} x^6 + \frac{14\,651}{30\,720} x^5 - \frac{3289}{61\,440} x^4 + \frac{759}{327\,860} x^3 \right),$$

$$u_{10}(x) = \sqrt{\frac{54\,185\,826\,156}{I_{24}}} \left(x^{12} - \frac{225}{44}x^{11} + \frac{1725}{154}x^{10} - \frac{2415}{176}x^9 + \frac{7245}{704}x^8 - \frac{13\,685}{2816}x^7 + \frac{4025}{2816}x^6 - \frac{22\,425}{90\,112}x^5 + \frac{1495}{65\,536}x^4 - \frac{1495}{1\,835\,008}x^3 \right),$$

where $x \equiv 1/(1 + a^2Q^2)$.

$$v_1(y) = \sqrt{\frac{1}{7\pi a^3}} \exp(-y)(y + 1),$$

$$v_2(y) = \sqrt{\frac{1}{3\pi a^3}} \exp(-y) \left(\frac{2}{3}y^2 - y - 1 \right),$$

$$v_3(y) = \sqrt{\frac{1}{385\pi a^3}} \exp(-y) \left(\frac{14}{3}y^3 - \frac{70}{3}y^2 + 15y + 15 \right),$$

$$v_4(y) = \sqrt{\frac{1}{1365\pi a^3}} \exp(-y) \left(4y^4 - 38y^3 + \frac{280}{3}y^2 - 35y - 35 \right),$$

$$v_5(y) = \sqrt{\frac{2}{77\pi a^3}} \exp(-y) \left(\frac{11}{45}y^5 - \frac{11}{3}y^4 - \frac{52}{3}y^3 - 28y^2 + 7y + 7 \right),$$

$$v_6(y) = \sqrt{\frac{2}{4641\pi a^3}} \exp(-y) \left(\frac{26}{45}y^6 - \frac{559}{45}y^5 + 93y^4 - 292y^3 + 350y^2 - 63y - 63 \right),$$

$$v_7(y) = \sqrt{\frac{1}{399\pi a^3}} \exp(-y) \left(\frac{2}{45}y^7 - \frac{58}{45}y^6 + \frac{623}{45}y^5 - 69y^4 + 162y^3 - 154y^2 + 21y + 21 \right),$$

$$v_8(y) = \sqrt{\frac{2}{19\,635\pi a^3}} \exp(-y) \left(\frac{68}{945}y^8 - \frac{170}{63}y^7 + \frac{352}{9}y^6 - \frac{2519}{9}y^5 + 1045y^4 - 1958y^3 + 1540y^2 - 165y - 165 \right),$$

$$v_9(y) = \sqrt{\frac{1}{72\,105\pi a^3}} \exp(-y) \left(\frac{38}{945}y^9 - \frac{170}{63}y^8 + \frac{248}{7}y^7 - \frac{3080}{9}y^6 + \frac{16\,522}{9}y^5 - 5478y^4 + 8536y^3 - 5720y^2 + 495y + 495 \right),$$

$$v_{10}(y) = \sqrt{\frac{1}{5005\pi a^3}} \exp(-y) \left(\frac{4}{2015}y^{10} - \frac{46}{405}y^9 + \frac{2522}{945}y^8 - \frac{10\,504}{315}y^7 + \frac{10\,868}{45}y^6 - \frac{46\,618}{45}y^5 + 2574y^4 - 3432y^3 + 2002y^2 - 143y - 143 \right),$$

where $y \equiv r/a$.

APPENDIX B

Basis function expansion with maximized entropy

As demonstrated in practical implementations of Fourier series or Taylor expansion, the total number of terms does not necessarily need to be exceedingly large if the series can converge quickly as the expansion term increases. As a result, high-order terms can be neglected. However, exactly how many expansion terms are required for data analysis varies from case to case. Alternatively, the constraint of maximized entropy can be imposed on the expansion. In statistical mechanics, this has been well recognized as an unbiased strategy to quantify the probability distribution with the inclusion of high-order contributions. In this mathematical context, the general form of $f(r)$ can be obtained by maximizing the following objective function:

$$H = -\langle \ln \tilde{f}(Q), \tilde{f}(Q) \rangle + \sum_n \lambda_n [\langle u_n(Q), \tilde{f}(Q) \rangle - a_n]. \quad (32)$$

To this end one can carry out the following functional derivatives over H with respect to $\tilde{f}(Q)$ and set it to zero, namely

$$0 = \frac{\delta H}{\delta \tilde{f}(Q)} = \left\langle -1 - \ln \tilde{f}(Q) + \sum_n \lambda_n u_n(Q), 1 \right\rangle. \quad (33)$$

It is straightforward to demonstrate that

$$\tilde{f}(Q) = \lambda_0 \exp \left[\sum_n \lambda_n u_n(Q) \right] \quad (34)$$

and

$$\left\langle \lambda_0 \exp \left[\sum_m \lambda_m u_m(Q) \right], u_n(Q) \right\rangle = a_n. \quad (35)$$

Likewise,

$$f(r) = \tilde{\lambda}_0 \exp \left[\sum_n \tilde{\lambda}_n v_n(r) \right] \quad (36)$$

and

$$\left\langle \tilde{\lambda}_0 \exp \left[\sum_n \tilde{\lambda}_n v_n(r) \right], v_n(r) \right\rangle = b_n, \quad (37)$$

where λ_0 and $\tilde{\lambda}_0$ are constants. Therefore, $\sqrt{n_m}F(Q)$ can be expressed as the functional form of $\lambda_0 \{ \exp[\sum_{n=1} \lambda_n u_n(Q)] - 1 \}$.

Acknowledgements

This research was supported by the Spallation Neutron Source, a US Department of Energy (DOE) Office of Science User Facility operated by Oak Ridge National Laboratory. This manuscript has been authored by UT-Battelle LLC, under contract DE-AC05-00OR22725 with the US DOE. The US government retains and the publisher, by accepting the article for publication, acknowledges that the US government retains a nonexclusive, paid-up, irrevocable worldwide license to publish or reproduce the published form of this manuscript, or allow others to do so, for US government purposes. DOE will provide public access to these results of federally sponsored research in accordance with the DOE Public Access Plan (<http://energy.gov/downloads/doe-publicaccess-plan> [**This URL gives a 'Page not found' error - please check!**]).

Funding information

Guan-Rong Huang is supported by the National Science and Technology Council (NSTC) in Taiwan (grant No. NSTC 111-2112-M-110-021-MY3). Yangyang Wang is supported by the US Department of Energy, Office of Science, Office of Basic Energy Sciences, Early Career Research Program (Award KC0402010) under Contract DE-AC05-00OR22725. Yuya Shinohara is supported by the US Department of Energy, Office of Science, Office of Basic Energy Sciences, Materials and Science and Engineering Division.

References

- Adelsberger, J., Kulkarni, A., Jain, A., Wang, W., Bivigou-Koumba, A. M., Busch, P., Pipich, V., Holderer, O., Hellweg, T., Laschewsky, A., Müller-Buschbaum, P. & Papadakis, C. M. (2010). *Macromolecules*, **43**, 2490–2501.
- Arfken, G. B., Weber, H. J. & Harris, F. E. (2012). *Mathematical Methods for Physicists: A Comprehensive Guide*. Amsterdam: Academic Press.
- Arnold, O., Bilheux, J., Borreguero, J., Buts, A., Campbell, S., Chapon, L., Doucet, M., Draper, N., Ferraz Leal, R., Gigg, M., Lynch, V., Markvardsen, A., Mikkelsen, D., Mikkelsen, R., Müller, R., Palmen, K., Parker, P., Passos, G., Perring, T., Peterson, P., Ren, S., Reuter, M., Savici, A., Taylor, J., Taylor, R., Tolchenov, R., Zhou, W. & Zikovsky, J. (2014). *Nucl. Instrum. Methods Phys. Res. A*, **764**, 156–166.
- Bang, J., Viswanathan, K., Lodge, T. P., Park, M. J. & Char, K. (2004). *J. Chem. Phys.* **121**, 11489–11500.
- Bergström, M. & Pedersen, J. S. (1999). *Phys. Chem. Chem. Phys.* **1**, 4437–4446.
- Brasher, L. L. & Kaler, E. W. (1996). *Langmuir*, **12**, 6270–6276.
- Cabane, B., Duplessix, R. & Zemb, T. (1985). *J. Phys. Fr.* **46**, 2161–2178.
- Castelletto, V., Hamley, I. W. & Pedersen, J. S. (2002). *J. Chem. Phys.* **117**, 8124–8129.
- Castelletto, V., Hamley, I. W. & Pedersen, J. S. (2004). *Langmuir*, **20**, 2992–2994.
- Chen, S.-H. (1986). *Annu. Rev. Phys. Chem.* **37**, 351–399.
- Chen, W.-R., Porcar, L., Liu, Y., Butler, P. D. & Magid, L. J. (2007). *Macromolecules*, **40**, 5887–5898.
- Choi, S.-H., Bates, F. S. & Lodge, T. P. (2009). *J. Phys. Chem. B*, **113**, 13840–13848.

- Dozier, W. D., Huang, J. S. & Fetters, L. J. (1991). *Macromolecules*, **24**, 2810–2814.
- Fermi, E. & Marshall, L. (1947). *Phys. Rev.* **71**, 666–677.
- Gapiński, J., Szymański, J., Wilk, A., Kohlbrecher, J., Patkowski, A. & Hołyst, R. (2010). *Langmuir*, **26**, 9304–9314.
- Glatter, O. (1977). *J. Appl. Cryst.* **10**, 415–421.
- Glatter, O. (2002). *Neutrons, X-rays and Light. Scattering Methods Applied to Soft Condensed Matter*, edited by P. Lindner & T. Zemb, ch. 4, pp. 73–102. Amsterdam: North-Holland.
- Goldmints, I., von Gottberg, F. K., Smith, K. A. & Hatton, T. A. (1997). *Langmuir*, **13**, 3659–3664.
- Goldmints, I., Yu, G.-E., Booth, C., Smith, K. A. & Hatton, T. A. (1999). *Langmuir*, **15**, 1651–1656.
- Grant, T. D. (2022). *J. Appl. Cryst.* **55**, 1116–1124.
- Hammouda, B. (2010a). *J. Appl. Cryst.* **43**, 716–719.
- Hammouda, B. (2010b). *Eur. Polym. J.* **46**, 2275–2281.
- Hansen, S. (2016). *J. Appl. Cryst.* **49**, 856–865.
- Hansen, S. & Pedersen, J. S. (1991). *J. Appl. Cryst.* **24**, 541–548.
- Hassan, P. A., Fritz, G. & Kaler, E. W. (2003). *J. Colloid Interface Sci.* **257**, 154–162.
- Hayter, J. B. & Zemb, T. (1982). *Chem. Phys. Lett.* **93**, 91–94.
- Heller, W. T., Cuneo, M., Debeer-Schmitt, L., Do, C., He, L., Heroux, L., Littrell, K., Pingali, S. V., Qian, S., Stanley, C., Urban, V. S., Wu, B. & Bras, W. (2018). *J. Appl. Cryst.* **51**, 242–248.
- Huang, G. R., Tung, C. H., Chang, D., Lam, C. N., Do, C., Shinohara, Y., Chang, S. Y., Wang, Y., Hong, K. & Chen, W. R. (2020). *J. Chem. Phys.* **153**, 184902.
- Huang, G., Tung, C., Porcar, L., Wang, Y., Shinohara, Y., Do, C. & Chen, W. (2023). *Macromolecules*, **56**, 6436–6443.
- Huang, G. R., Wang, Y., Do, C., Porcar, L., Shinohara, Y., Egami, T. & Chen, W. R. (2019). *J. Phys. Chem. Lett.* **10**, 3978–3984.
- Jensen, G. V., Lund, R., Gummel, J., Monkenbusch, M., Narayanan, T. & Pedersen, J. S. (2013). *J. Am. Chem. Soc.* **135**, 7214–7222.
- König, N., Willner, L., Pipich, V., Zinn, T. & Lund, R. (2019). *Phys. Rev. Lett.* **122**, 078001.
- Kumi, B. C., Hammouda, B. & Greer, S. C. (2014). *J. Colloid Interface Sci.* **434**, 201–207.
- Laurati, M., Stellbrink, J., Lund, R., Willner, L., Zaccarelli, E. & Richter, D. (2007). *Phys. Rev. E*, **76**, 041503.
- Li, X., Hong, K., Liu, Y., Shew, C. Y., Liu, E., Herwig, K. W., Smith, G. S., Zhao, J., Zhang, G., Pispas, S. & Chen, W. R. (2010). *J. Chem. Phys.* **133**, 144912.
- Likos, C. N., Löwen, H., Poppe, A., Willner, L., Roovers, J., Cubitt, B. & Richter, D. (1998). *Phys. Rev. E*, **58**, 6299–6307.
- Liu, Y., Baglioni, P., Teixeira, J. & Chen, S. H. (1994). *J. Phys. Chem.* **98**, 10208–10215.
- Liu, Y., Chen, C.-Y., Chen, H.-L., Hong, K., Shew, C. Y., Li, X., Liu, L., Melnichenko, Y. B., Smith, G. S., Herwig, K. W., Porcar, L. & Chen, W. (2010). *J. Phys. Chem. Lett.* **1**, 2020–2024.
- Liu, Y., Chen, S.-H. & Huang, J. (1996). *Phys. Rev. E*, **54**, 1698–1708.
- Liu, Y., Chen, S.-H. & Huang, J. (1998). *Macromolecules*, **31**, 2236–2244.
- Ma, Y. & Lodge, T. P. (2016). *Macromolecules*, **49**, 3639–3646.
- Manet, S., Lecchi, A., Impéror-Clerc, M., Zholobenko, V., Durand, D., Oliveira, C. L. P., Pedersen, J. S., Grillo, I., Meneau, F. & Rochas, C. (2011). *J. Phys. Chem. B*, **115**, 11318–11329.
- Mao, G., Sukumaran, S., Beaucage, G., Saboungi, M.-L. & Thiyagarajan, P. (2001). *Macromolecules*, **34**, 552–558.
- Marshall, W. G. & Lovesey, S. W. (1971). *Theory of Thermal Neutron Scattering: The Use of Neutrons for the Investigation of Condensed Matter*. Oxford: Clarendon Press.
- Moore, P. B. (1980). *J. Appl. Cryst.* **13**, 168–175.
- Pedersen, J. S. (1994). *J. Appl. Cryst.* **27**, 595–608.
- Pedersen, J. S. (2000). *J. Appl. Cryst.* **33**, 637–640.
- Pedersen, J. S. & Gerstenberg, M. C. (1996). *Macromolecules*, **29**, 1363–1365.
- Pedersen, J. S., Svaneborg, C., Almdal, K., Hamley, I. W. & Young, R. N. (2003). *Macromolecules*, **36**, 416–433.

1,255	Poppe, A., Willner, L., Allgaier, J., Stellbrink, J. & Richter, D. (1997). <i>Macromolecules</i> , 30 , 7462–7471.	1,312
1,256	Provencher, S. (1976). <i>J. Chem. Phys.</i> 64 , 2772–2777.	1,313
1,257	Ramzi, A., Prager, M., Richter, D., Efstratiadis, V., Hadjichristidis, N., Young, R. N. & Allgaier, J. B. (1997). <i>Macromolecules</i> , 30 , 7171–7182.	1,314
1,258	Sheu, E. Y. & Chen, S.-H. (1988). <i>J. Phys. Chem.</i> 92 , 4466–4474.	1,315
1,259	Stellbrink, J., Niu, A., Allgaier, J., Richter, D., Koenig, B. W., Hartmann, R., Coates, G. W. & Fetters, L. J. (1995). <i>Macromolecules</i> , 28 , 8829–8834.	1,316
1,260	Stieger, M., Pedersen, J. S., Lindner, P. & Richtering, W. (2004). <i>Langmuir</i> , 20 , 7283–7292.	1,317
1,261	Svensson, B., Olsson, U., Alexandridis, P. & Mortensen, M. (1999). <i>Macromolecules</i> , 32 , 6725–6733.	1,318
1,262	Svergun, D. I. (1992). <i>J. Appl. Cryst.</i> 25 , 495–503.	1,319
1,263	Svergun, D. I., Feigin, L. A. & Schedrin, B. M. (1982). <i>Acta Cryst. A</i> 38 , 827–835.	1,320
1,264	Tung, C., Huang, G., Chang, S., Han, Y., Chen, W. & Do, C. (2020). <i>J. Phys. Chem. Lett.</i> 11 , 7334–7341.	1,321
1,265	Vad, T. & Sager, W. F. C. (2011). <i>J. Appl. Cryst.</i> 44 , 32–42.	1,322
1,266	Wang, E., Lu, J., Bates, F. S. & Lodge, T. P. (2018). <i>Macromolecules</i> , 51 , 3563–3571.	1,323
1,267	Willner, L., Jucknischke, O., Richter, D., Farago, B., Fetters, L. J. & Huang, J. S. (2000a). [Please complete full details for reference - original was identical to Willner et al. (2000b)]	1,324
1,268	Willner, L., Poppe, A., Allgaier, J., Monkenbusch, M., Lindner, P. & Richter, D. (2000b). <i>Europhys. Lett.</i> 51 , 628–634.	1,325
1,269	Yang, L. & Alexandridis, P. (2000). <i>Langmuir</i> , 16 , 4819–4829.	1,326
1,270	Yang, L., Alexandridis, P., Steytler, D. C., Kositzka, M. J. & Holzwarth, J. F. (2000). <i>Langmuir</i> , 16 , 8555–8561.	1,327
1,271	Yip, S. (2015). <i>Nuclear Radiation Interactions</i> . New Jersey: World Scientific.	1,328
1,272	Zemb, T. & Charpin, P. (1985). <i>J. Phys. Fr.</i> 46 , 249–256.	1,329
1,273	Zhao, D., Ma, Y. & Lodge, T. P. (2018). <i>Macromolecules</i> , 51 , 2312–2320.	1,330
1,274	Zhao, J. K., Gao, C. Y. & Liu, D. (2010). <i>J. Appl. Cryst.</i> 43 , 1068–1077.	1,331
1,275		1,332
1,276		1,333
1,277		1,334
1,278		1,335
1,279		1,336
1,280		1,337
1,281		1,338
1,282		1,339
1,283		1,340
1,284		1,341
1,285		1,342
1,286		1,343
1,287		1,344
1,288		1,345
1,289		1,346
1,290		1,347
1,291		1,348
1,292		1,349
1,293		1,350
1,294		1,351
1,295		1,352
1,296		1,353
1,297		1,354
1,298		1,355
1,299		1,356
1,300		1,357
1,301		1,358
1,302		1,359
1,303		1,360
1,304		1,361
1,305		1,362
1,306		1,363
1,307		1,364
1,308		1,365
1,309		1,366
1,310		1,367
1,311		1,368